

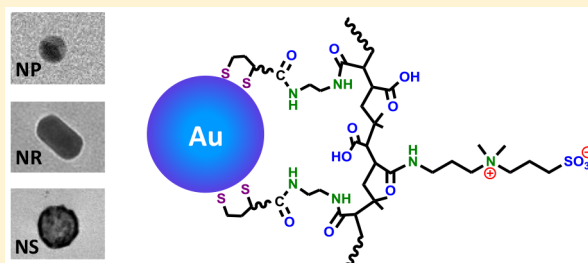
Enhanced Colloidal Stability of Various Gold Nanostructures Using a Multicoordinating Polymer Coating

Wentao Wang,[†] Xin Ji,[†] Liang Du, and Hedi Mattoussi*[✉]

Department of Chemistry and Biochemistry, Florida State University, 95 Chieftan Way, Tallahassee, Florida 32306, United States

Supporting Information

ABSTRACT: We describe the effectiveness of a multicoordinating polymer coating to surface functionalize gold nanospheres, nanoshells, and nanorods and promote their steric stabilization in biological media. The polymer ligand synthesized via one-step nucleophilic addition reaction starting with poly(isobutylene-*alt*-maleic anhydride) precursor presents multiple lipoic acid groups for strong coordination on metal-rich surfaces and several hydrophilic motifs (e.g., zwitterion groups or short poly(ethylene glycol) (PEG) chains) to promote water solubilization. We show that nanocrystals ligated with this polymer are compact in size and exhibit excellent long-term colloidal stability over broad conditions. We compare the ability of zwitterion- and PEG-modified polymer ligands to shield the metal surfaces from sodium cyanide digestion, or resist the competitive removal by dithiothreitol (DTT). We find that polymers appended with either hydrophilic motif essentially eliminate DTT competition for surface binding, while nanocrystals capped with the PEGylated coating exhibits substantially better resistance to sodium cyanide digestion compared with zwitterionic coating. Furthermore, we probe the differences between the two coatings in terms of endowing surface charge to the nanocrystals and affecting their Brownian diffusion properties. Additionally, we show that zwitterionic coating is very effective in preventing the formation of protein corona on such nanostructures, a highly valuable result with direct implications in biotechnology.



INTRODUCTION

Nanocrystals made of gold and silver cores exhibit several surface plasmon resonance (SPR) absorption properties that can be tuned by controlling their size and/or shape.^{1–3} For instance, spherical gold nanoparticles with a diameter smaller than ~50 nm exhibit a single SPR peak at ~520 nm with size-dependent extinction coefficients.⁴ In comparison, the absorption spectra of gold nanorods exhibit an additional longitudinal SPR peak that shifts toward the near-infrared (NIR) regime with increasing aspect ratio.^{4,5} The strong longitudinal absorption permits easy excitation of these materials with NIR laser sources, efficiently generating localized heat.^{3,5} These nanostructures can also interact with proximal molecules (e.g., dyes), where they act as either strong fluorescence quencher or enhancer depending on the separation distance.^{6,7} These properties coupled with a size range comparable to that of biomolecules make them attractive for use in biological sensor design and therapeutic/diagnostic applications.^{1,3,5,8–14} Their effective integration into biology hinges on the ability to develop surface functionalization approaches that provide nanocrystals with robust colloidal stability and compact dimensions, while endowing them with specific targeting properties.^{9,15,16}

Cap exchange with coordinating ligands is an effective strategy for fine-tuning the surface properties of a variety of inorganic nanocrystals.^{11,15,17} Because of the strong Au-to-thiol coordination, thiolated ligands (e.g., derivatives of dihydroliipoic

acid, DHLA) have been widely used for the surface modification of gold nanoparticles.^{18–21} Moreover, to provide gold nanocrystals with long-term colloidal stability while reducing nonspecific absorption of proteins, incorporating high molecular weight poly(ethylene glycol) (e.g., PEG₅₀₀₀) as the hydrophilic motif in the ligand has often been used as the method of choice.^{19,22,23} This tends to substantially increase the hydrodynamic volume of the hydrophilic nanocrystals. To reduce the overall dimensions while maintaining aqueous solubility, thiol-based ligands appended with compact zwitterion groups have been developed.^{18,24,25} However, using molecular-scale ligands and/or ligands with low coordination numbers to promote the long-term colloidal stability of large gold nanospheres and nanorods has remained a great challenge. This is further compounded by the fact that under ambient conditions most thiolated ligands are prone to oxidative desorption from the nanoparticle surfaces.^{5,26,27} Such problems seriously affect the stability of nanocrystal dispersions at very low concentrations, where higher dissociation rates tend to take place.²⁸ The advent of multicoordinating polymer ligands can alleviate the above issues. With their multicoordinating interactions, these ligands can reduce the dissociation rates, thus enhancing the binding affinity to the nanocrystal

Received: August 3, 2017

Revised: September 21, 2017

Published: September 25, 2017

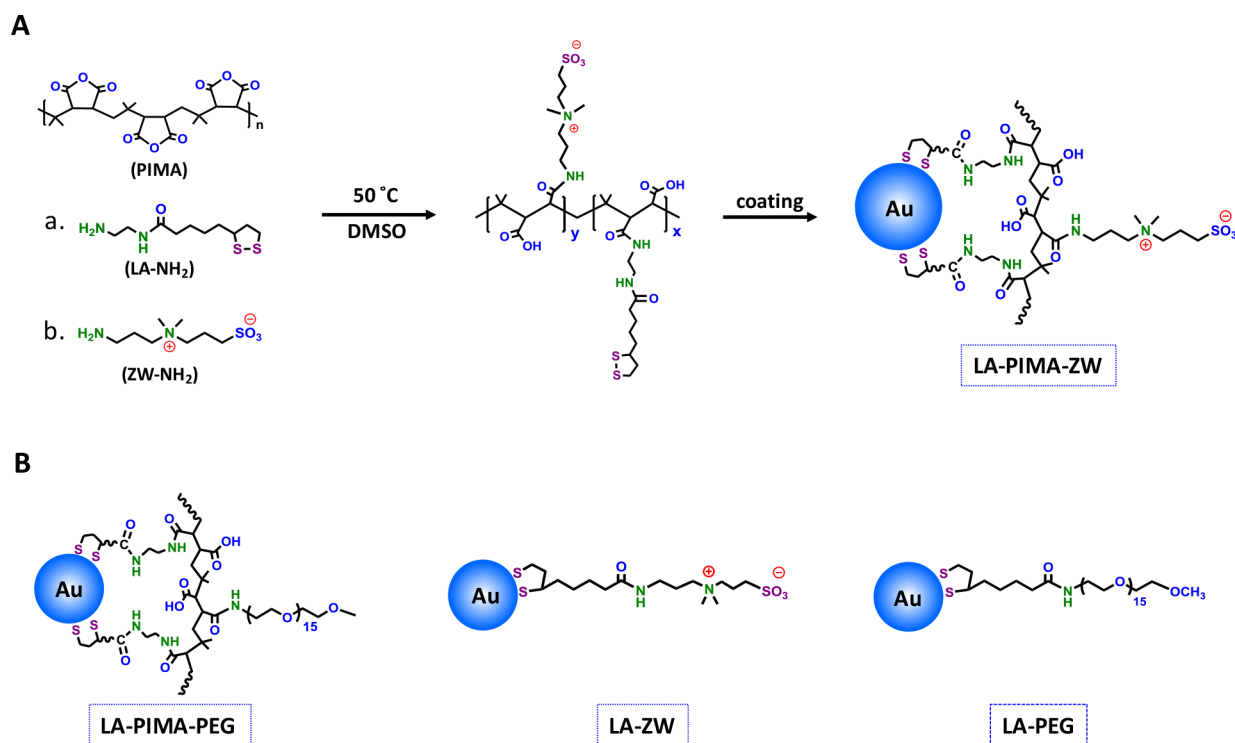


Figure 1. (A) Schematic representation of the synthetic scheme employed for preparing the lipoic acid- and zwitterion-modified polymer ligand, LA-PIMA-ZW, using one-step nucleophilic addition reaction, along with a representation of a LA-PIMA-ZW-coated AuNP. (B) Other representative nanocrystal surface coatings used in this study, LA-PIMA-PEG, LA-ZW, and LA-PEG.

surfaces.^{28–33} A few recent studies have shown that capping gold nanorods (over 100 nm in length) with PEG-modified polymer yields excellent long-term colloidal stability.^{30,33–35}

In this study, we introduce a multicoordinating zwitterion-rich polymer as a ligand ideally suited for the surface functionalization of gold nanocrystals, namely, gold nanospheres (NPs), gold nanoshells (NSs), and gold nanorods (NRs). The ligand presents multiple lipoic acid anchors for metal coordination and several zwitterion moieties for water solubilization. Coating with this ligand yields nanocrystals that are compact and exhibit long-term colloidal stability over a broad range of biological conditions. This zwitterionic ligand also drastically reduces the nonspecific adsorption of proteins. We characterize the colloidal stability of these polymer-capped nanocrystals using a combination of analytical techniques including optical absorption spectroscopy, transmission electron microscopy (TEM), agarose gel electrophoresis, and dynamic light scattering (DLS). We also compare ligands presenting the zwitterion motifs with the ones modified with short PEG chains (as shown in Figure 1). In particular, we probe differences between the abilities of zwitterionic and PEG coatings to impart surface charge, affect the diffusion behavior, and protect the metallic core from sodium cyanide digestion and competition from dithiothreitol.

EXPERIMENTAL SECTION

Ligand Synthesis. We focus on the synthesis of one representative polymer ligand made of 50% lipoic acid (LA) and 50% zwitterion (ZW), LA-PIMA-ZW. In a 50 mL three-neck round-bottom flask, 0.385 g of poly(isobutylene-*alt*-maleic anhydride) (PIMA, MW ~ 6000 g/mol, 2.5 mmol of monomer units) was dissolved in 5 mL of dimethyl sulfoxide (DMSO). The solution was purged with nitrogen and heated to 50 °C

using an oil bath. LA-NH₂ (0.31 g, 1.25 mmol) dissolved in 1 mL of DMSO was added to the PIMA solution through a syringe, followed by addition of 1 mL of DMSO solution containing amino-zwitterion, ZW-NH₂ (0.280 g, 1.25 mmol). The reaction mixture was left stirring at 50 °C overnight. The content was concentrated to ~1 mL under vacuum, then 30 mL of acetone was added to precipitate the compound. Following one round of centrifugation, the solid pellet was collected, washed two times with chloroform, and then dried under vacuum, yielding the final product as a yellow solid, with a reaction yield of ~87%. Additional details on the synthesis of precursors (i.e., LA-NH₂ and ZW-NH₂) and other ligands, namely, LA-PIMA-PEG polymer, LA-PEG, and LA-ZW are summarized in the Supporting Information and previous reports.^{28,36,37}

Growth of Gold Nanoparticles. Citrate-stabilized gold nanospheres (~14 nm in diameter as measured by TEM) were prepared following the method developed by Turkevich and co-workers.³⁸ Briefly, HAuCl₄ (50 mM, 5 mL) was added to a boiling aqueous solution of sodium citrate (1.7 mM, 500 mL) and left stirring for 15 min. The reaction mixture was then cooled to room temperature. The nanoparticles were purified from excess unreacted reagents and concentrated using a centrifugal filtration device (Millipore, MW cutoff = 50 kDa).

Growth of Gold Nanoshells. The gold nanoshells (~18 nm in diameter) were prepared following the protocol reported by Zhang and co-workers.³⁹ Briefly, a solution (2 L total volume) made of deionized water mixed with 11 mL of 0.5 M sodium citrate and 4 mL of 0.4 M cobalt chloride was purified from oxygen by bubbling ultrahigh purity argon gas for ~30 min. Rapid injection of freshly prepared sodium borohydride solution (~10 mL, 2 M) under vigorous stirring initiated the growth of cobalt nanospheres. The clear, slightly pinkish

solution turned brown after sodium borohydride reduction, indicating the formation of cobalt nanoparticles. The solution was left at room temperature for ~30–45 min (no stirring) under argon flow until the complete hydrolysis of the sodium borohydride. The cobalt nanoparticle dispersion was then quickly transferred to a vortexing solution made from 2 L of deionized water containing ~800 μL of 0.1 M chloroauric acid. Rapid reduction of the gold precursors by cobalt NPs resulted in deposition of a gold layer on the nanoparticles. At the same time, the cobalt NP cores were oxidized to cobalt oxide. Further exposing the solution to air promoted the complete oxidation and dissolution of the cobalt cores, leaving empty gold nanoshells. The gold nanoshell dispersion was centrifuged at 14 000 rpm for 20 min, the solvent was decanted, and the resulting pellet was resuspended in deionized water. The process was repeated twice, and the final sample was stored for further use.

Growth of Gold Nanorods. The gold nanorods used in this study (45 nm \times 19 nm) were prepared following the scheme initially developed by Murray and co-workers using seeded growth in binary surfactant mixtures of cetyltrimethylammonium bromide and sodium salicylate (CTAB/NaSa).⁴⁰ The seed solution was prepared as follows: 5 mL of 0.5 mM HAuCl_4 was mixed with 5 mL of 0.2 M CTAB solution in a 20 mL scintillation vial. Fresh NaBH_4 solution (0.6 mL, 0.01 M) was diluted with deionized (DI) water to 1 mL, and the mixture was injected into the above Au(III)–CTAB solution under vigorous stirring (1200 rpm); the stirring was stopped after 2 min. This seed solution was “aged” at room temperature for 30 min before use. The growth solution was prepared separately by dissolving 9.0 g of CTAB and 0.8 g of NaSa in 250 mL of warm water (~50 $^\circ\text{C}$) using a 1 L Erlenmeyer flask. The solution was cooled to 30 $^\circ\text{C}$, and 6 mL of 4 mM AgNO_3 solution was added. The mixture was kept undisturbed at 30 $^\circ\text{C}$ for 15 min, after which HAuCl_4 solution (250 mL, 1 mM) was added. After stirring at 400 rpm for 15 min, 1 mL of 0.064 M ascorbic acid was added followed by vigorously stirring for 30 s. Finally, 0.8 mL of seed solution was injected into the flask. The resulting mixture was stirred for 30 s and left undisturbed at 30 $^\circ\text{C}$ for 12 h to allow for growth and homogenization of the nanorods. The materials were isolated by centrifugation at 7000 rpm for 30 min and removal of the supernatant. The nanorods were resuspended in DI water.

Ligand Exchange. We limit the description to ligand exchange of citrate-capped nanoparticles with LA-PIMA-ZW ligand. The same protocol was applied to gold nanoshells and nanorods. Briefly, 10 mg of LA-PIMA-ZW was dissolved in 2 mL of phosphate buffer (pH 8, 50 mM). An aliquot of gold nanoparticle dispersion (~6 nM, 2 mL) was slowly added to the ligand solution, and the mixture was left under continuous stirring overnight at 50 $^\circ\text{C}$. The nanoparticle dispersion was filtered through a 0.45 μm syringe filter, and excess free ligands were removed by applying three rounds of concentration/dilution with DI water using a centrifugal filtration device (Millipore, MW cutoff = 50 kDa).

Gel Electrophoresis and Protein Corona Tests. Gel electrophoresis experiments were run on 0.6% agarose gel using Tris borate EDTA buffer (TBE, 89 mM Tris, 89 mM boric acid, 1 mM EDTA). For colloidal stability tests and surface charge comparison, the stock dispersions of gold nanospheres, nanoshells, and nanorods were diluted to 8, 4, and 1.5 nM with DI water, respectively. The dispersions were mixed with 2 μL of loading buffer made of Ficoll 400 immediately prior to

use; the total loading volume was 20 μL . The gel was run for 30 or 60 min using a voltage of 5.5 V/cm, and then white light images were captured using a Nikon D3000 camera.

For the protein corona tests, the stock dispersion of each set of nanocrystals was mixed with different volumes of bovine serum albumin (BSA) solutions in Eppendorf tubes and then diluted with phosphate buffer (pH 7, 20 mM). The final concentrations were 8 nM for AuNPs, 4 nM for AuNSs, and 1.5 nM for AuNRs. The concentration of BSA in these samples was varied from 0 to 50 mg/mL. The mixtures were incubated for 1 h at room temperature and then mixed with 2 μL of loading buffer made of Ficoll 400 immediately prior to gel electrophoresis measurements; the total loading volume was 20 μL . The gels were run under a voltage of 5.5 V/cm for 30 min, and then imaged under white light exposure.

Dynamic Light Scattering: Background. Dynamic light scattering relies on the analysis of the time-dependent scattered laser signal intensity, $I(q, \tau)$, due to Brownian motion of the solute objects in the medium (in this case the nanocrystals in the dispersion).⁴¹ τ and q respectively designate the delay time and the scattering wavevector (i.e., scattering angle θ). Analysis of the scattered intensity and its dependence on time and scattering angle provides a measure of the solute diffusion coefficient. Experimentally, the autocorrelation function of the scattered intensity $I(q, \tau)$ is defined as^{42,43}

$$g^{(2)}(\tau, q) = \frac{\langle I(q, t) I(q, t + \tau) \rangle}{\langle I(q, t) \rangle^2} \quad (1)$$

where $\langle \dots \rangle$ denotes the average over time and the scattering wavevector is expressed as $q = \frac{4\pi n}{\lambda} \sin\left(\frac{\theta}{2}\right)$. From this one can extract a measure of the electric field autocorrelation function defined as

$$g^{(1)}(\tau, q) = a(\lg^{(2)}(\tau, q) - 1)^{1/2} \quad (2)$$

where a is an experimental constant proportional to the amplitude of the scattered signal. For solutions of homogeneous colloidal nanoparticles, polymers, proteins, etc. with a given size dispersity and in the dilute regime (i.e., isolated solute objects), $g^{(1)}(\tau, q)$ deviates from an ideal single exponential decay (predicted for a monodisperse nanoparticle dispersion). Instead it is commonly fit to a cumulants series:

$$g^{(1)}(\tau, q) = a \exp\left(-\Gamma\tau + \frac{\mu_2}{2}\tau^2 + \dots\right) \quad (3)$$

where Γ and μ_2 designate the first and second cumulants. Γ corresponds to the decay rate expressed in terms of the scattering wavevector, q , and the apparent translational diffusion coefficient, D_{app} , as

$$\Gamma = D_{\text{app}} q^2 \quad (4)$$

The ratio μ_2/Γ^2 is the polydispersity index, PDI (defined as size distribution width/mean size), which reflects the effects of inhomogeneities in the sample, attributed among others to size heterogeneity. Plotting Γ versus q^2 yields a linear curve, where the slope is the apparent diffusion coefficient of the scattering nanoparticles. The measured D_{app} also accounts for the internanoparticle interactions in the medium and can be simplified to⁴²

$$D_{\text{app}} = D_0(1 + k_d c) \quad (5)$$

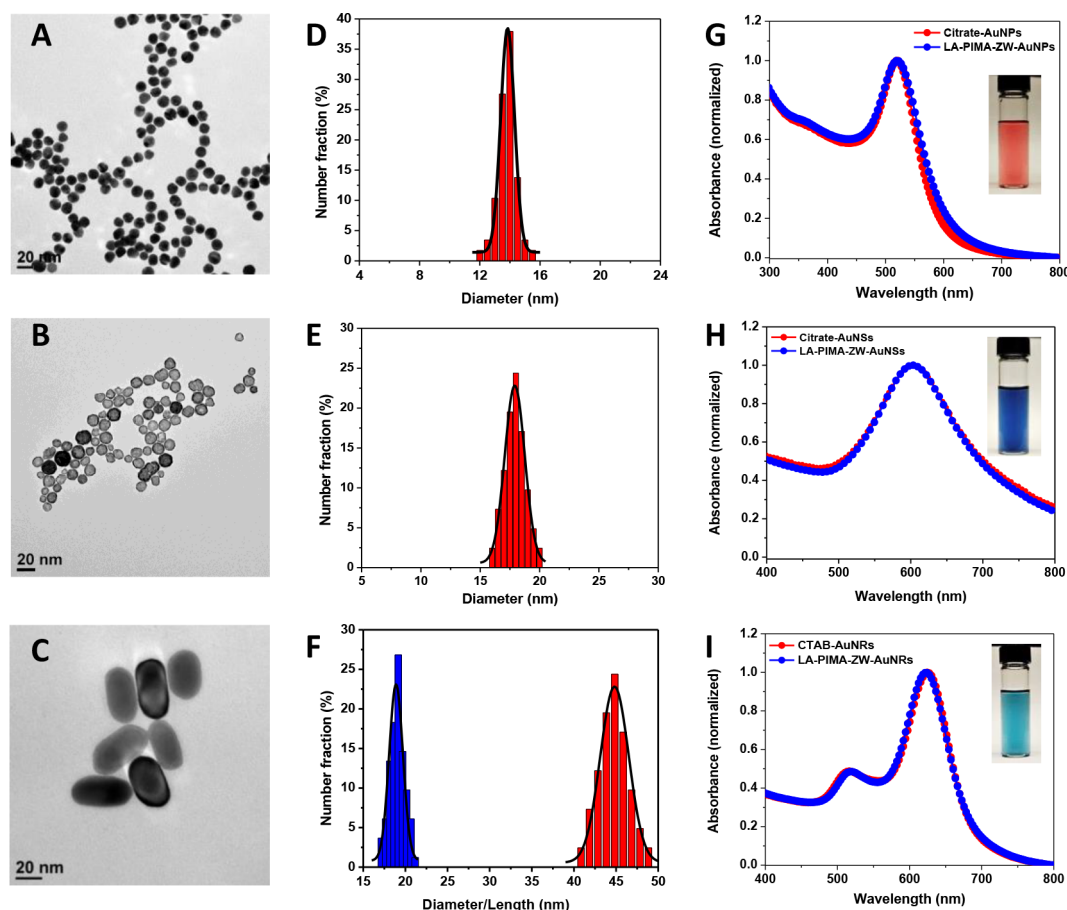


Figure 2. (A–C) TEM images of LA-PIMA-ZW-capped gold nanospheres, nanoshells, and nanorods. (D–F) Size distribution histograms of polymer-coated gold nanospheres ($D \sim 14$ nm), nanoshells ($D \sim 18$ nm), and nanorods ($L \times D$: ~ 45 nm \times 19 nm). (G–I) UV–vis absorption spectra of various gold nanocrystals before and after ligand exchange with LA-PIMA-ZW. Insets show white light images of three sets of LA-PIMA-ZW-coated nanocrystals dispersed in water.

where the interaction parameter, k_d , depends among others on the second virial coefficient, A_2 , and c is the NP concentration.^{41,44,45} When $k_d > 0$, it indicates that repulsive stabilizing interparticle interactions dominate the medium, while $k_d < 0$ implies that destabilizing interactions dominate; the latter may indicate early stages of aggregation buildup. Extrapolation of D_{app} at concentration $c = 0$ yields a measure for the diffusion coefficient of single nanoparticles, D_0 . If combined with the Stokes–Einstein relation, it can provide an accurate measure for the hydrodynamic radius ($R_{H,0}$) of a single nanoparticle in the medium:

$$R_{H,0} = \frac{kT}{6\pi\eta D_0} \quad (6)$$

where k is the Boltzmann constant, T is the temperature in kelvin, and η is the solvent viscosity.

Sodium Cyanide Digestion Test. NaCN solution (80 μ L, 0.5 M) was loaded into a quartz cuvette (0.2 cm \times 1 cm, optical path = 1 cm). The solution was diluted with deionized water; then the desired volume of AuNP stock solution was swiftly added to the cuvette and mixed thoroughly. The amount of DI water added was adjusted so that the final volume was 800 μ L. For each experiment, the final concentrations of AuNPs and NaCN were 1 nM and 50 mM, respectively. The first absorption spectrum was recorded within 30 s of mixing followed by collecting an absorption spectrum every 4 min.

Dithiothreitol (DTT) Stability Test. DTT solution (400 μ L, 2 M) was mixed with NaCl solution (240 μ L, 1 M) in a quartz cuvette (0.2 cm \times 1 cm, optical path = 1 cm) and further diluted with H₂O before addition of the desired volume of AuNP/AuNR dispersion; the total volume of the dispersion was 800 μ L. The AuNP or AuNR dispersion was rapidly added to the NaCl/DTT aqueous solution and mixed thoroughly. An initial absorption spectrum was collected within 30 s after mixing followed by recording an absorption spectrum every 3 min. The final concentrations of DTT and NaCl were 1 M and 300 mM, respectively, while the final concentrations of AuNPs and AuNRs were 1 and 0.1 nM.

RESULTS AND DISCUSSION

Rationale. Our approach is centered on the premise that a polymer ligand presenting several thiolate anchors and zwitterion hydrophilic moieties should be more effective for coating metal nanostructures even with rather large surface areas (e.g., nanorods) than molecular-scale mono- or bidentate ligands. The synthesis of the polymer ligand, LA-PIMA-ZW, used in this study relies on the nucleophilic addition reaction to modify a short poly(isobutylene-*alt*-maleic anhydride), PIMA, with hydrophilic zwitterion (ZW) groups and lipoic acid (LA) anchors, as schematically shown in Figure 1. This yields a coordinating polymer laterally appended, via amide bonds, with several lipoic acid groups for strong coordination on the nanocrystal surface, along with compact zwitterion moieties for

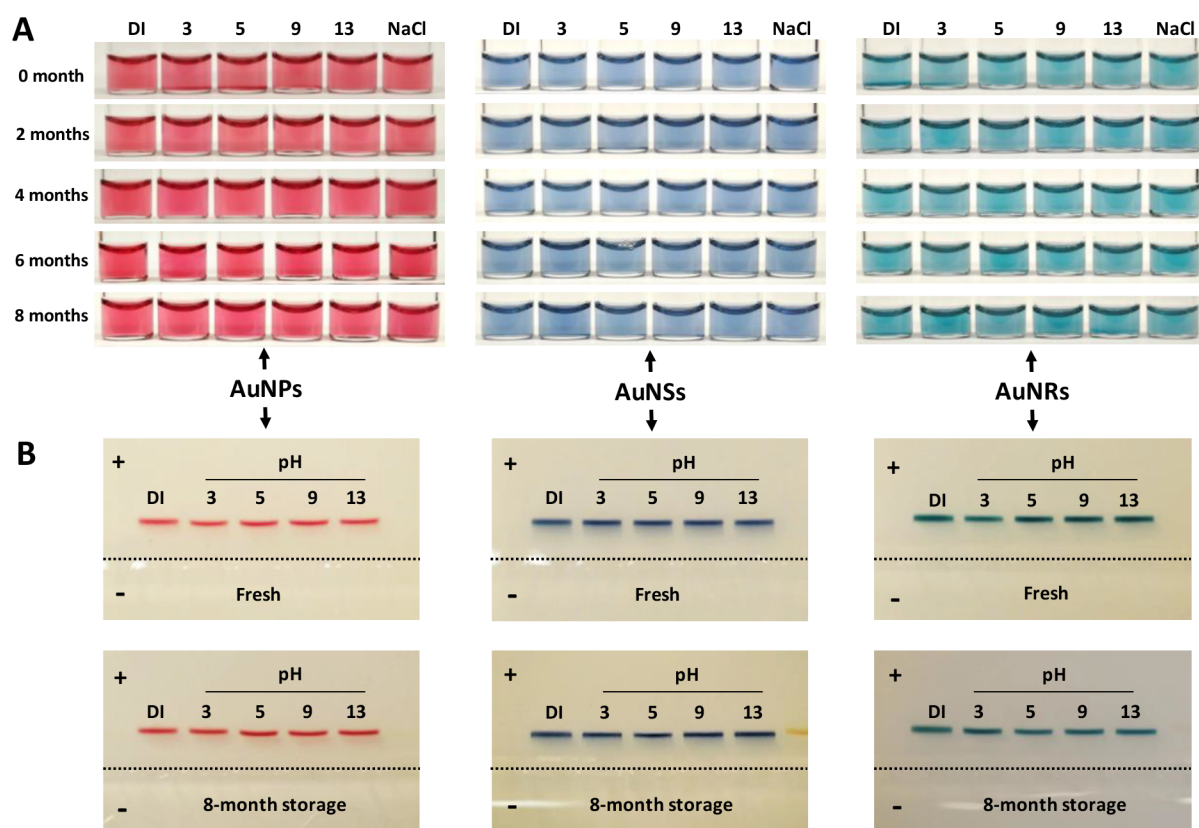


Figure 3. Colloidal stability tests applied to polymer-coated Au nanocrystals. (A) White light images of dispersions of AuNPs, AuNSs, and AuNRs coated with LA-PIMA-ZW dispersed in phosphate buffer (20 mM) over the pH range from 3 to 13 and in the presence of 1 M NaCl. (B) Agarose gel electrophoresis images of AuNPs, AuNSs, and AuNRs ligated with LA-PIMA-ZW dispersed in buffers over the pH range 3–13. The top panels represent freshly prepared samples, while the bottom panels show the images collected from those samples after 8 months of storage. The dashed line indicates the location of the loading wells. Gels were run at 5.5 V/cm for 30 min.

water solubilization. The ligand also presents several carboxyl groups freed during the ring opening reaction, which are hydrophilic and reactive. The ligand architecture can be tuned by controlling the molar ratio of each amine-containing precursor with respect to the maleic anhydride rings in the PIMA chain. In this study, the ratio of lipoic acid to zwitterion was limited to 50:50, which is expected to yield ~ 20 anchoring groups and ~ 20 hydrophilic moieties per ligand.²⁸ We should emphasize that this synthetic scheme can be easily applied to prepare other types of ligands, such as PEGylated polymer (e.g., LA-PIMA-PEG, see Figure 1).^{28,37,46}

Three different gold nanostructures have been used to test the effectiveness of the designed polymer: (1) Citrate-stabilized spherical gold nanoparticles, AuNPs, with average diameter of ~ 14 nm were prepared following the route introduced by Turkevich and co-workers.⁴⁷ (2) Gold nanoshells, AuNSs, with diameter of ~ 18 nm were grown on cobalt seeds as previously described in refs 39 and 48. (3) Gold nanorods (~ 45 nm \times 19 nm), AuNRs, were prepared by seeded-mediated growth in binary surfactant mixtures of cetyltrimethylammonium bromide (CTAB) and sodium salicylate.⁴⁰ Representative TEM images show that the nanocrystals exhibit uniform size and shape with reduced dispersity (see Figure S1). Because of differences in the resonance features (i.e., resonance bands and absorption wavelengths), dispersions of these gold nanocrystals exhibit distinct colors.^{39,40} For instance, dispersions of nanoshells and nanorods with low aspect ratio appear blue, while those of spherical gold nanoparticles are reddish.

Characterization of the Hydrophilic Nanocrystals.

Following ligand exchange with LA-PIMA-ZW, the purified hydrophilic nanocrystals were characterized using TEM and UV–visible absorption spectroscopy, and supplemented with ^1H NMR spectroscopy.

The TEM images combined with the size distribution histograms, shown in Figure 2, indicate that nanocrystals capped with LA-PIMA-ZW maintain their overall size, with no sign of aggregation or change in the overall shape. The absorption spectra of these nanocrystals exhibit features essentially identical with those collected from the starting materials (Figure 2), implying that the integrity of the various nanocrystals following phase transfer has been preserved. The polymer-ligated nanoparticles were further characterized using pulsed-field gradient-based water suppression ^1H NMR spectroscopy. Spectra collected from the polymer-ligated AuNPs and AuNRs as well as from the precursors LA-NH₂ and ZW-NH₂ are provided in the Supporting Information, Figures S2–S4. A typical spectrum of LA-PIMA-ZW-capped AuNP or AuNR dispersions shows several broadened but distinct peaks at ~ 1.1 – 1.9 ppm, attributed to protons characteristic of the lipoic acid groups; these chemical shifts are consistent with the signatures of the precursor LA-NH₂. The spectrum also shows a pronounced resonance at 3.0 ppm corresponding to the methyl groups of the zwitterion moieties, while the broad peak at ~ 0.9 ppm is ascribed to the methyl protons of the PIMA backbone. These data clearly indicate that the native capping molecules

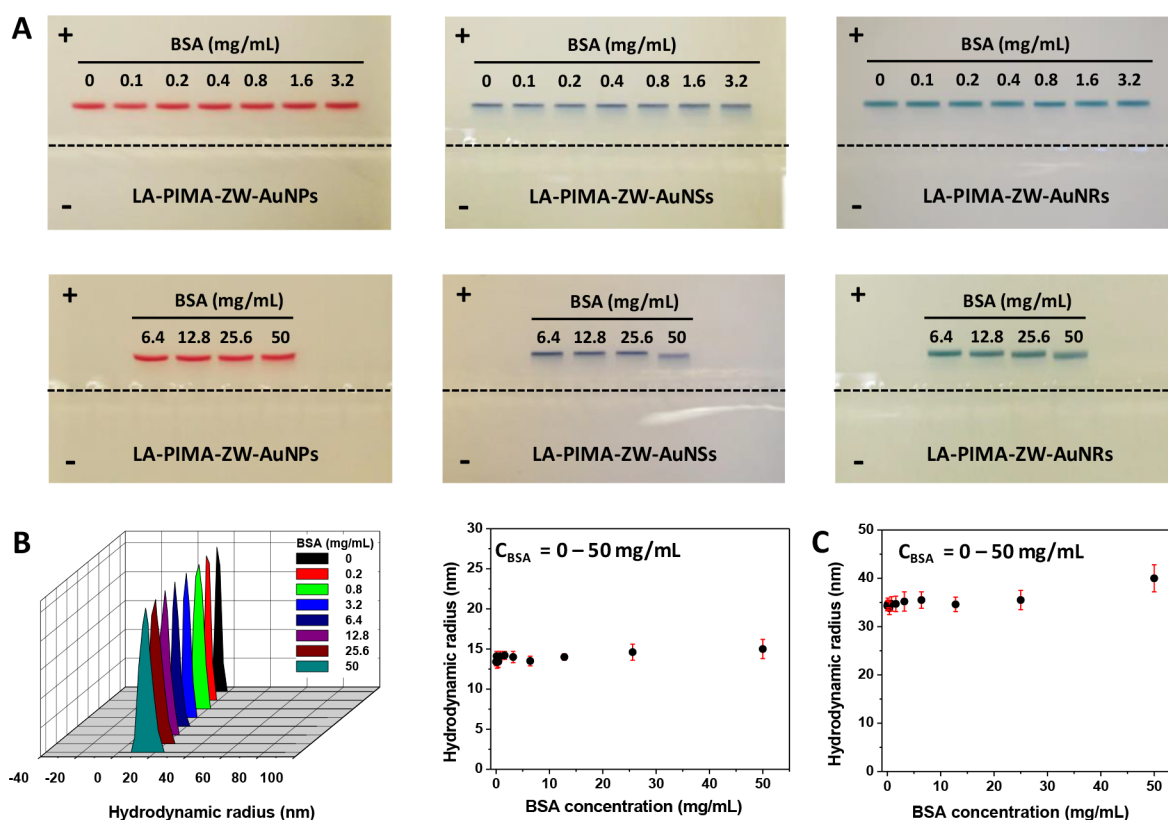


Figure 4. Protein corona tests. (A) Agarose gel electrophoresis images of LA-PIMA-ZW-capped AuNPs (left), AuNSs (middle), and AuNRs (right) after incubation with different concentrations of BSA (0–50 mg/mL) for 1 h. (B) Histogram of hydrodynamic size distribution extracted from DLS measurements, applied to LA-PIMA-ZW-AuNP dispersions that have been incubated with BSA over the concentration range from 0 to 50 mg/mL. Essentially identical size distribution profiles were extracted, with $R_H \cong 13 \pm 1$ nm. (C) Progression of hydrodynamic size of AuNSs following incubation with BSA (0–50 mg/mL). The hydrodynamic radius was essentially unchanged, albeit a slight increase of ~ 5 nm was measured at 50 mg/mL BSA.

have essentially been completely substituted by the coordinating polymers during ligand exchange.

Colloidal Stability Tests. Figure 3A shows white light images of LA-PIMA-ZW-capped nanospheres, nanoshells, and nanorods dispersed in buffers in the pH range 3–13 and in the presence of 1 M NaCl. All dispersions stayed stable for at least 8 months of storage, with no sign of degradation or aggregate buildup. These stability tests were further complemented with agarose gel electrophoresis measurements. As shown in Figure 3B, narrow and homogeneous migration bands with little to no smearing were measured for each set of hydrophilic nanocrystals dispersed in different pH buffers, either freshly prepared or after 8 months of storage. Additionally, we note that the polymer-coated nanocrystals have migrated toward the anode, a result that reflects a homogeneous size distribution of nanocrystals with net negative surface charge; the latter is attributed to the combined contributions from several carboxylic groups along the polymer backbone and sulfobetaine groups in the hydrophilic motifs (see section on Surface Charge).

Protein Adsorption Tests: Reduced Nonspecific Interactions. Effective integration of a variety of nanoprobosc (e.g., gold nanoparticles) in biomedicine has been hampered by low targeting efficiency and unfavorable biodistribution.^{49–52} This is primarily attributed to the nonspecific protein adsorption on the nanocrystal surfaces, particularly when exposed to biological fluids.^{24,51,53,54} Such protein adsorption can severely alter the nanoparticle's physical properties

including in vivo diffusion coefficient and circulation lifetime. It can also compromise the targeting efficiency toward specific receptors.⁵⁰ Thus, engineering “nonsticky” surfaces with no protein adsorption is crucial for better integration of these materials into biology and nanomedicine.

To test the ability of our polymer coating to prevent protein adsorption on the nanocrystals, we used a simple yet sensitive measurement based on probing changes in the gel electrophoretic mobility of the nanocrystals when exposed to high concentrations of proteins. A few previous studies have reported that buildup of an adsorbed protein layer (often referred to as “protein corona”) on the nanoparticle surfaces can alter the mobility shift and band shape.⁵² In this study, three sets of nanocrystals ligated with LA-PIMA-ZW were evaluated in the presence of bovine serum albumin (BSA), a protein routinely used in model studies of protein adsorption onto nanoparticles.⁵⁵ The BSA concentration was varied from 0 to 50 mg/mL, a value close to the highest concentration of serum albumin found in the human blood (35–50 mg/mL).⁵⁶ Following incubation with BSA, the dispersions were loaded onto agarose gel and run at 5.5 V/cm for 30 min. The images in Figure 4A show that narrow bands with essentially identical mobility shifts were measured for each set of nanocrystals over the range of BSA concentrations used, although a slightly smaller shift was observed for dispersions of nanoshells and nanorods mixed with 50 mg/mL BSA. Gel electrophoresis data were further confirmed by tracking changes in the hydrodynamic radius extracted from dynamic light scattering (DLS)

measurements. These measurements were limited to spherical nanocrystals (i.e., nanoparticles and nanoshells); the shape anisotropy of gold nanorods makes the use of DLS not very sensitive in this case. The collected data show that, when the concentration of BSA increased from 0 to 50 mg/mL, the hydrodynamic radius of the spherical nanoparticles essentially stayed constant ($R_H \cong 13 \pm 1$ nm, Figure 4B). Similar results were measured for gold nanoshells except that the hydrodynamic size increased by ~ 5 nm at 50 mg/mL BSA, indicating the presence of weak interactions between polymer-coated nanoshell and BSA at the highest concentration (Figure 4C). These results are consistent with the gel electrophoresis data. The above data combined confirm that zwitterion coating provides Au nanocrystals with uniform size and surface charge distribution along with “nonsticky” surface properties, which greatly reduces protein adsorption on the nanocrystals. Similar results have been observed for Au nanocrystals ligated with PEG-modified polymers, LA-PIMA-PEG.³⁵

Comparing the Nature and Effectiveness of Zwitterion and PEG Coatings. An important question to address is how nanocrystals capped with ligands presenting the zwitterion motif compare with those presenting PEG moieties in terms of achieving colloidal stability, endowing surface charge, affecting the Brownian diffusion properties, and the ability to shield the metallic cores from the surrounding medium. Our ligand design provides a flexible platform where the properties of the two hydrophilic motifs can be directly compared. A side-by-side comparison of the behavior of Au nanocrystals ligated with LA-PIMA-ZW and LA-PIMA-PEG was carried out with emphasis on three main aspects: (1) gel mobility and effects of surface charges; (2) nanoparticle diffusion properties and hydrodynamic size; (3) resistance to sodium cyanide digestion. We also investigated the effects of ligand coordination number on the colloidal stability of the nanocrystals in aqueous solutions by comparing the above polymer coatings to bidentate ligands (LA-PEG and LA-ZW) against competition from dithiothreitol.

Surface Charge. We probed differences in the overall surface charge endowed by the zwitterion-appended and PEG-modified polymer coatings by comparing the mobilities of the nanocrystals functionalized with either polymer using agarose gel electrophoresis measurements. The gel images in Figure 5A,B show a side-by-side comparison of the mobility shifts measured for the three sets of nanocrystals ligated with either LA-PIMA-PEG or LA-PIMA-ZW polymer; the gels were run for 30 and 60 min at 5.5 V/cm. The mobility data indicate that, though both polymers yield nanocrystals with a negative surface charge, a larger net negative charge was measured for LA-PIMA-ZW coating. This implies that, in addition to the charges provided by the carboxy groups on the polymer backbone, zwitterion moieties contribute extra net negative charges to the nanocrystals. This result is consistent with the gel data collected from luminescent quantum dots functionalized with these two coatings.⁵⁷ It is also worth noting that, though similar mobility shifts were measured for the different types of nanocrystals coated with LA-PIMA-PEG, small differences were observed when LA-PIMA-ZW coating was used. Similar data were collected after 8 months of storage, as shown in Figure 5C. This difference in mobility shift measured for the LA-PIMA-ZW-coated nanocrystals may be attributed to variations in the overall surface area, shape, and net surface-charge density presented on each set of nanocrystals.

Brownian Diffusion and Hydrodynamic Radius. We characterized the diffusion properties of gold nanocrystals

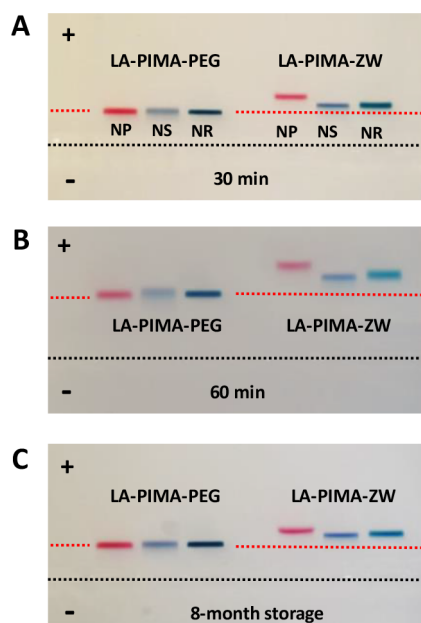


Figure 5. Side-by-side comparison of gel mobility shifts for AuNPs, AuNSs, and AuNRs coated with LA-PIMA-PEG (left) and LA-PIMA-ZW (right). The gels were run at 5.5 V/cm run for (A) 30, (B) 60, and (C) 30 min after 8 months of storage. The black dashed line indicates the location of the loading wells.

capped with LA-PIMA-ZW and LA-PIMA-PEG in the dilute regime using dynamic light scattering measurements. For each sample with a given nanocrystal concentration, we measured the autocorrelation function, $g^{(1)}(\tau, \theta)$, at several scattering angles between 40 and 140° using an average over three runs of 10 s each. Figure 6 shows representative plots of $\log(g^{(1)}(\tau))$ vs τ and $g^{(1)}(\tau)$ vs $\log \tau$, collected from dispersions of LA-PIMA-ZW-AuNPs (Figure 6A,B) and LA-PIMA-PEG-AuNPs (Figure 6E,F) at six different scattering angles. A very good fit to the data using second-order cumulants (eq 3, Experimental Section) was found, indicating that the dispersions are homogeneous with narrow size distribution. The plots of decay rate Γ (the first cumulant) versus q^2 shown in Figure 6C,G are linear, as expected from eq 4 for homogeneous nanoparticle dispersions in the dilute regime and at small scattering angles.⁴¹ Additionally, the dependence of the apparent diffusion coefficient (D_{app} , extracted from the slope of Γ vs q^2) on the concentrations is linear with a positive slope, implying that repulsive stabilizing interactions between the nanoparticles dominate in both cases (see Figure 6D,H).

From extrapolation to zero concentration, we extract a measure for the diffusion coefficient of individual nanoparticles, $D_0 = 17.08 \mu\text{m}^2 \text{s}^{-1}$ for LA-PIMA-ZW coating and $D_0 = 12.44 \mu\text{m}^2 \text{s}^{-1}$ for LA-PIMA-PEG coating. Combining this D_0 with the Stokes–Einstein relation (eq 6, Experimental Section) provides a measure for the hydrodynamic radius for individual nanoparticles: $R_{H,0} \sim 12.9$ nm for LA-PIMA-ZW-AuNPs and $R_{H,0} \sim 16.9$ nm for LA-PIMA-PEG-AuNPs. Clearly, the zwitterion coating provides a smaller radius, as expected given the relative larger lateral extension of the PEG moieties compared with the zwitterion groups.

We next compared the apparent hydrodynamic radius ($R_{H,app}$) of the nanoparticles before and after ligand exchange with the two polymer coatings. Figure 6I shows representative plots of the autocorrelation function collected from dispersions

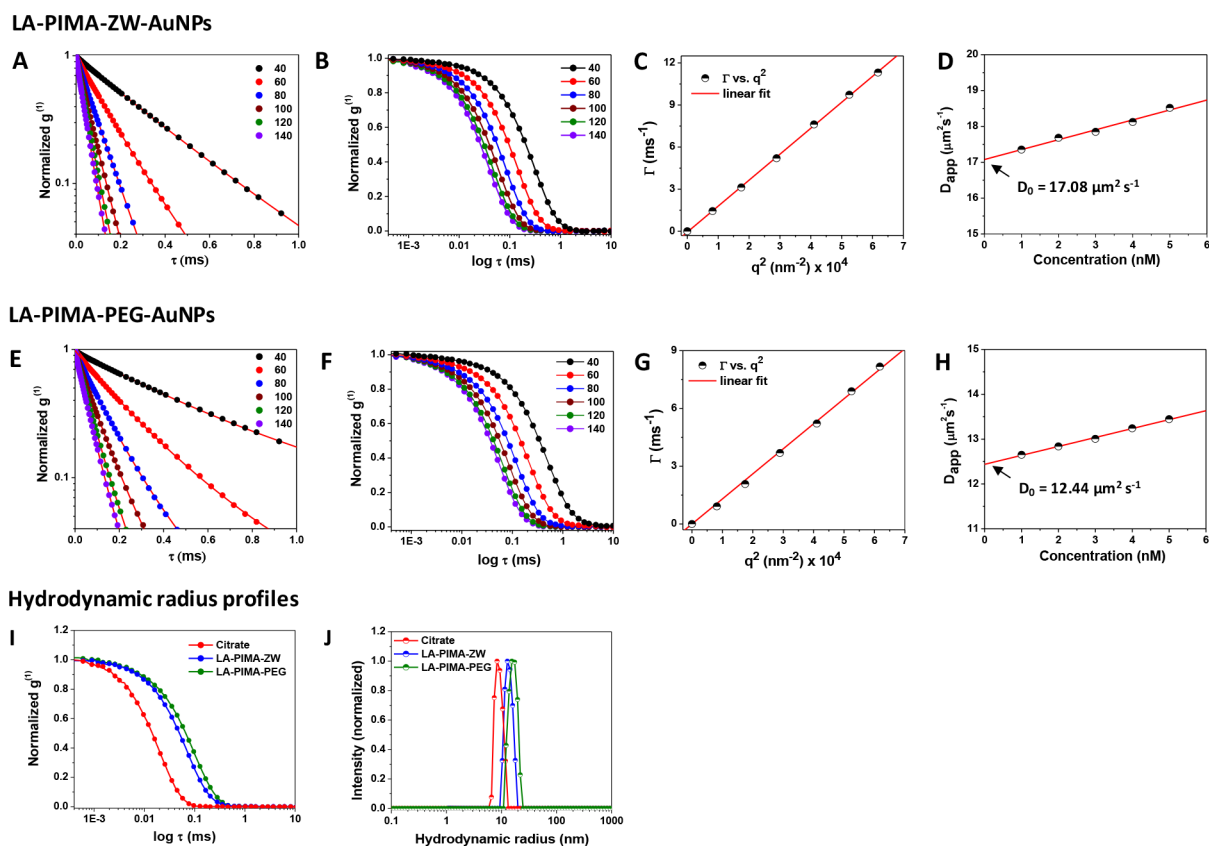


Figure 6. Dynamic light scattering measurements. (A, B) Representative profiles of normalized autocorrelation function, $\log(g^{(1)}(\tau))$ vs τ and $g^{(1)}(\tau)$ vs $\log \tau$, respectively, collected from LA-PIMA-ZW-AuNP dispersions at various scattering angles in the range 40–140°, along with second order cumulant fits. $g^{(1)}(\tau)$ were normalized with respect to the value at $\tau = 0$. (C) Plot of decay rate Γ versus q^2 , together with a linear fit using eq 4. (D) Apparent diffusion coefficient (D_{app}) versus concentration, along with a linear fit. (E–H) Similar set of data was collected and analyzed for LA-PIMA-PEG capped AuNPs. (I) Representative plots of $g^{(1)}(\tau)$ vs $\log \tau$, collected from dispersions of AuNPs before and after ligand exchange with the LA-PIMA-ZW and LA-PIMA-PEG. (J) Histogram of hydrodynamic size distribution extracted from the Laplace transform of the autocorrelation functions collected from dispersions of (red) citrate, (blue) LA-PIMA-ZW, and (green) LA-PIMA-PEG capped AuNPs.

of AuNPs before and after ligand exchange with LA-PIMA-ZW (blue profile) and LA-PIMA-PEG (green profile). Plots of the intensity vs hydrodynamic size histograms extracted from the Laplace transform of $g^{(1)}(\tau, q)$,⁴¹ shown in Figure 6J, indicate that both coatings provide aggregate-free nanocrystal dispersions with low polydispersity index values ($\text{PDI} \leq 0.1$). The DLS data also indicate that ligand exchange using these polymers increases the overall size of the nanocrystals: $R_{H,app} \sim 8.3$ nm for citrate-capped AuNPs, $R_{H,app} \sim 12.0$ nm for LA-PIMA-ZW-capped AuNPs, and $R_{H,app} \sim 15.5$ nm for LA-PIMA-PEG-AuNPs. Nonetheless, the zwitterion coating yields more compact overall size as discussed above. Note that $R_{H,app}$ is slightly smaller than $R_{H,0}$, an expected result for sterically stabilized NP dispersions.^{35,41}

Similar analysis was applied to the DLS data collected from LA-PIMA-ZW-capped gold nanoshells (see Supporting Information, Figure S5). These data slightly differ from those collected from AuNPs above. For instance, the value extracted for nanoshells $R_{H,0} \sim 35.8$ nm (calculated using $D_0 = 6.15 \mu\text{m}^2 \text{s}^{-1}$) is ~ 3 times larger than that measured for AuNPs (see above), although their core sizes measured by TEM are close. Additionally, the size distribution profiles extracted from the Laplace transform of $g^{(1)}(\tau)$ for nanoshells stabilized with either LA-PIMA-ZW or LA-PIMA-PEG coatings are comparable. This may be attributed to differences in the contributions of the

hydrodynamic interactions to the Brownian motion experienced by hollow nanoshells compared with solid nanoparticles.

NaCN Digestion Tests. This test probes the ability of the surface coating to “protect” the metallic core against etching by sodium cyanide ions. When cyanide anions come in contact with the metallic cores, they form complexes with the gold atoms, progressively etching the nanoparticle surfaces. This converts the reddish AuNP dispersions into a colorless solution of $\text{Au}(\text{CN})_2^-$ ions. This test has been used to study the effects of coordination number on the colloidal stability of different size nanoparticles.^{58,59} Here, we utilized the test to probe the effects of varying the nature and coordination number of the capping ligands on their ability to shield the metal cores against etching by the surrounding ions. We compare the shielding provided by PEG and ZW motifs in both polymeric and molecular-scale ligands: LA-PIMA-ZW vs LA-PIMA-PEG and LA-ZW vs LA-PEG.

Figure 7A,B shows the time progression of the absorption spectra collected from AuNP dispersions (1 nM concentration) capped with LA-PIMA-ZW and LA-PIMA-PEG following the addition of 50 mM NaCN. The absorption spectra were acquired at 4 min intervals. Data show that there is a progressive and steady decrease in the absorption profiles with time for both samples. However, the changes were drastically different from one set of ligands to another. In particular, the decay in the plasmonic peak with time was much

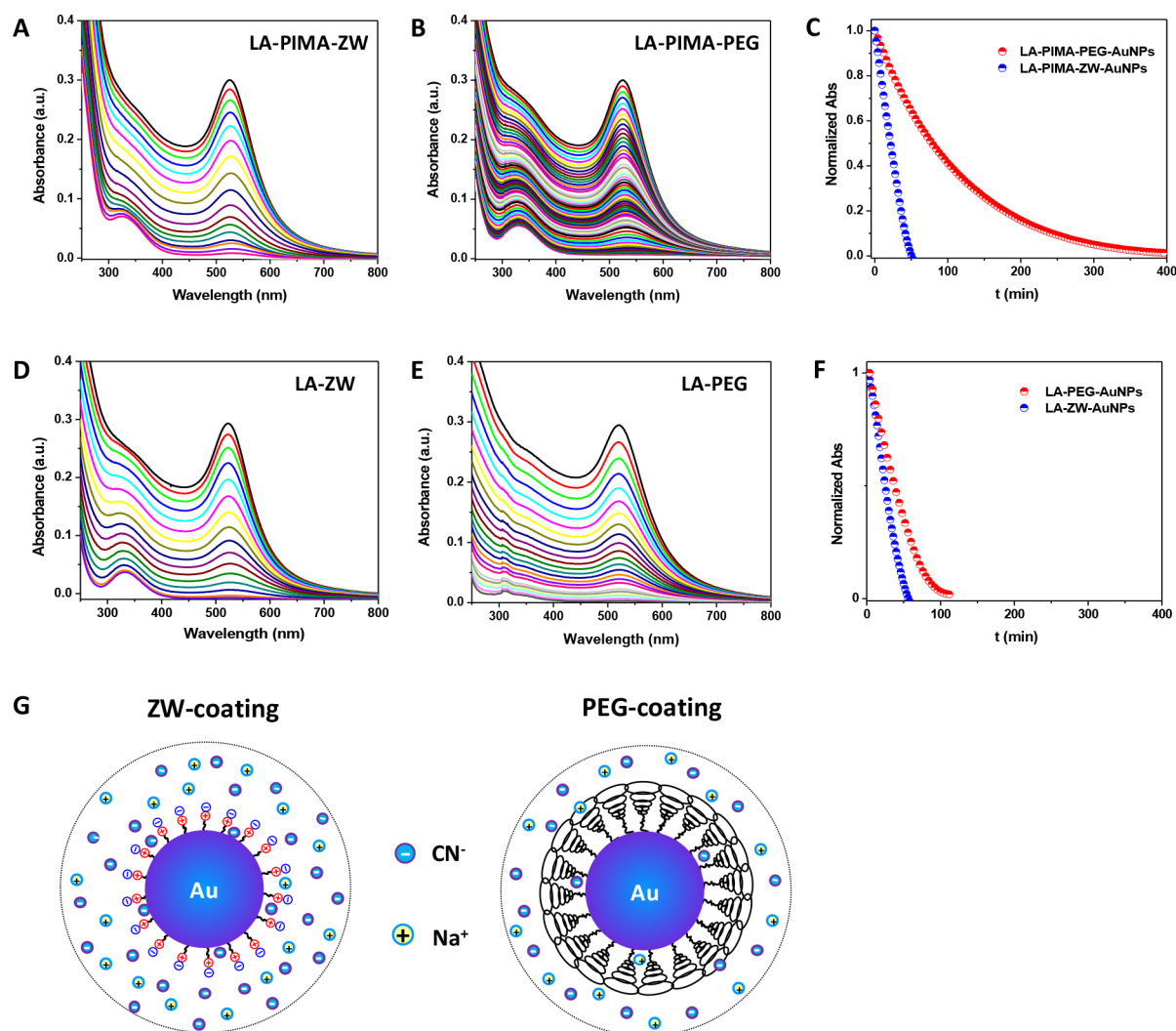


Figure 7. Time progression of absorption spectra collected from 1 nM AuNPs in the presence of 50 mM sodium cyanide with four distinct surface coatings: (A) LA-PIMA-ZW, (B) LA-PIMA-PEG, (D) LA-ZW, and (E) LA-PEG. (C, F) Normalized absorbance of AuNPs at the SPR peak (~ 520 nm), extracted from the data plotted in panels A/B and D/E. (G) Schematic representation of the shielding effects provided by PEG vs zwitterion coatings against sodium cyanide etching.

slower for LA-PIMA-PEG-AuNPs compared with LA-PIMA-ZW-AuNPs, indicating rather different digestion kinetics of the NPs depending on the capping ligand. The rate of decomposition was assessed by measuring the time-dependent decrease in the SPR peak and fitting it to a first-order exponential decay function in the form^{58,59}

$$A = A_0 e^{(-t/t_d)} \quad (7)$$

where A_0 is the absorbance value at $t = 0$ min and t_d designates the decay constant; the latter reflects the ability of the capping ligand to prevent etching of the NPs by cyanide ions when the other parameters are fixed (e.g., NaCN and AuNP concentrations). The progression of the normalized absorbance at ~ 520 nm for AuNPs are shown in Figure 7C, where the LA-PIMA-PEG-AuNPs exhibited a slower digestion rate ($t_d = 108$ min) than their zwitterionic analogue ($t_d = 22$ min). Smaller differences in the digestion kinetics are collected from AuNPs coated with the bidentate monomer ligands, as shown in Figure 7D–F, where the decay time for LA-PEG-AuNPs ($t_d = 38.3$ min) is ~ 1.6 times longer than that of LA-ZW-AuNPs ($t_d = 23.9$ min); note that the t_d values extracted for LA-PEG-AuNPs

are comparable to those reported for similar size AuNPs.⁵⁸ These results clearly indicate that PEG coating provides a better protection against etching by cyanide ions. This result can be attributed to the packing of PEG coils on the nanoparticle surfaces, resulting in more effective shielding of the metallic cores as schematically depicted in Figure 7G. Compared with the rather small, rigid, and charged zwitterion motif, such a close-packed “mushroom” structure formed by the PEG moieties can effectively limit access of cyanide ions to the gold surface. Moreover, the shielding effects are drastically enhanced when a multicoordinating PEG-modified polymer is used.

Stability against DTT Competition. Ligand-to-nanoparticle coordination affinity is a crucial factor that determines the colloidal stability of nanoparticles in aqueous media or organic solvents. It has been shown that ligands presenting dithiol anchors exhibit higher affinity to AuNPs than their monothiolate counterparts.⁵⁸ Here, we probe the effects of increasing the coordination number of ligands, modified with either PEG or zwitterionic motifs, on the colloidal stability of AuNPs and AuNRs in the presence of competitive binding from DTT. At high concentration, DTT can competitively displace the

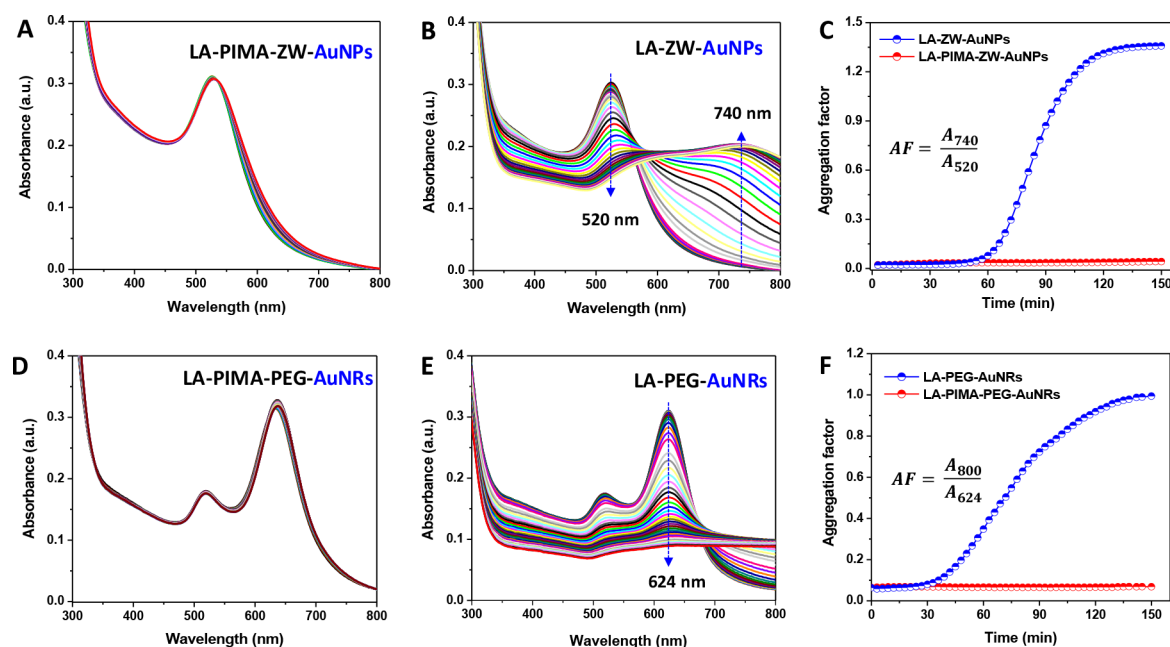


Figure 8. DTT competition tests. Time progression of UV–vis absorption spectra collected from 14 nm AuNPs capped with LA-PIMA-ZW (A) and LA-ZW (B); AuNRs (45 nm × 19 nm) capped with LA-PIMA-PEG (D) and LA-PEG (E). (C, F) Aggregation factor (AF) of AuNPs and AuNRs extracted from the data in panels A/B and D/E. Data consistently show that the multicoordinating polymer capping provides stronger resistance to DTT competition compared to those measured for the bidentate ligands, independent of the nanocrystal structure.

capping ligands from the AuNP surface, resulting in progressive aggregation buildup. DTT competition is also more rapid in the presence of excess salt because of enhanced screening effects.^{58,60} As the competitive removal of the surface ligands alters the spectroscopic properties of the dispersion, the strength of ligand coordination onto the nanoparticle can be experimentally tested by tracking changes in the dispersion absorption spectra with time.

Figure 8A shows the time-dependent progression of the absorption spectra collected from LA-PIMA-ZW-AuNP dispersion (~1 nM) containing 1 M DTT and 300 mM NaCl. The spectra exhibit little to no change, indicating no sign of aggregate buildup. In control experiments, spectra collected from dispersions of LA-ZW-AuNPs show a significant change with time, manifesting in a decrease in the plasmon band at ~520 nm along with an increase in the absorbance at longer wavelengths, as shown in Figure 8B. The increase at ~740 nm reflects the nanoparticle-to-nanoparticle association and aggregation induced by DTT competition. To quantify this competition, we track the progression of the aggregation factor defined as the ratio between the optical densities at 740 and 520 nm ($AF = \text{Abs}_{740}/\text{Abs}_{520}$), because changes in the absorption spectra due to aggregation were most noticeable at these two wavelengths in our experiments.⁵⁸ If the ligand affinity to the nanoparticle is strong, AF should remain either unaltered or exhibit small change with time. In contrast, the nanoparticles become unstable and AF will increase with time if DTT can rapidly displace the capping ligands. Figure 8C shows a side-by-side comparison of the progression of AF with time for dispersions of LA-PIMA-ZW-AuNPs (red dots) and LA-ZW-AuNPs (blue dots). Data show that a negligible aggregation factor was measured for the polymer-coated NPs throughout the duration of the test, whereas the increase in AF was sizable after 60 min for AuNPs coated with the LA-ZW ligand, indicating that macroscopic aggregation has taken place.

Similar differences were recorded between AuNPs capped with LA-PIMA-PEG and with LA-PEG (data not shown).

The DTT stability test has also been applied to AuNRs. The comparison centered on PEGylated ligands: LA-PIMA-PEG versus LA-PEG. Similar to what was measured for AuNPs, we found that LA-PIMA-PEG-AuNRs stayed stable and aggregate-free in the presence of DTT (Figure 8D,F). In contrast, pronounced changes were measured for LA-PEG-AuNR dispersions within 30 min, where a decrease in the absorption profiles for both longitudinal and transverse resonance peaks coupled with an increase in the absorption at longer wavelength (>700 nm) were recorded, see Figure 8E,F. We also examined the colloidal stability of AuNRs coated with zwitterionic ligands against DTT competition. The LA-PIMA-ZW coating provided strong resistance to DTT competition, albeit with a slight decrease in the longitudinal plasmon resonance peak (see Supporting Information, Figure S6). In contrast, we found that ligand exchange of AuNRs with LA-ZW failed to reproducibly provide stable dispersions, as precipitation of the NRs often built up during ligand exchange. This implies that these rather small size ligands do not confer enough entropy-driven steric stabilization to the nanorods (due to their rather large surface areas), compared to PEG-modified lipoic acid or the multi-coordinating polymers.

These data combined clearly show that nanocrystals ligated with polymers presenting multidentate anchors exhibit stronger resistance to DTT competition than those capped with monomeric bidentate ligands. They suggest that the dominant factor in the ligand capacity to provide stable Au nanocrystals against competition from small coordinating molecules is the number of coordinating groups, as this defines the strength of the ligand binding to the metal surfaces.

CONCLUSION

We have shown the effectiveness of a multicoordinating polymer ligand to surface functionalize three different types

of gold nanocrystals (nanospheres, nanorods and nanoshells) and promote their long-term stability in biological media. The polymer is prepared via nucleophilic addition reaction by simultaneously modifying a short poly(isobutylene-*alt*-maleic anhydride) with multiple lipoic acid anchoring groups that ensure strong coordination onto the metal surfaces, along with several zwitterion or PEG motifs for buffer compatibility. This coating strategy yields nanocrystals that are compact in size and exhibit excellent colloidal stability over a broad range of conditions, while drastically reducing nonspecific protein adsorption in biological media. We have applied various analytical techniques (e.g., dynamic light scattering, agarose gel electrophoresis and optical spectroscopy) to investigate differences between zwitterion and PEG coatings on the nanocrystal properties with respect to net surface charge, Brownian diffusion properties, and the ligand's ability to protect the metallic core from etching by sodium cyanide. We also tested the capacity of these polymer ligands compared to their monomer counterparts (i.e., high and low coordination), to provide colloidal stability against competition from excess DTT. Overall, we found that polymer coating presenting the zwitterion motif reduces the hydrodynamic size and provides effective resistance against competition by DTT, but has limited effect against sodium cyanide digestion. PEGylated polymer ligands, in comparison, provide better protection from cyanide digestion, while maintaining great resistance to DTT competition. In addition to the nanocrystals tested here, other metallic nanostructures including Au nanostars and silver nanocrystals could be functionalized with this coating approach. These polymer-coated gold nanostructures are greatly promising for use in biology and nanomedicine. They could be easily tested in a variety of biological demonstrations ranging from sensor design and cellular/tissue imaging to photothermal therapy.

We should emphasize that the current chemical scheme and surface functionalization strategy is applicable to a variety of nanomaterials, such as those made of semiconducting and magnetic cores by simply changing the anchoring groups. In addition, the synthetic scheme used here allows the easy introduction of various functional groups, providing platforms that are readily adapted for bioorthogonal conjugation. It can also allow the insertion of specific biomolecules within the ligand structures *in situ*.⁵⁷

■ ASSOCIATED CONTENT

5 Supporting Information

The Supporting Information is available free of charge on the ACS Publications website at DOI: 10.1021/acs.jpcc.7b07732.

Additional information and data on materials, instrumentation, TEM images of nanocrystals prior to ligand exchange, NMR spectra of lipoic acid amine, zwitterion amine, LA-PIMA-ZW-AuNPs, and LA-PIMA-ZW-AuNRs, and DLS profiles of nanoshells (PDF)

■ AUTHOR INFORMATION

Corresponding Author

*E-mail: mattoussi@chem.fsu.edu.

ORCID

Wentao Wang: 0000-0003-2273-4171

Hedi Mattoussi: 0000-0002-6511-9323

Present Address

†W.W. and X.J.: Ocean Nanotech, LLC, 7964 Arjons Dr., San Diego, CA 92126.

Notes

The authors declare no competing financial interest.

■ ACKNOWLEDGMENTS

The authors thank FSU, the National Science Foundation (NSF-CHE Nos. 1508501 and 1058957), and Asahi-Kasei for financial support. They also thank Goutam Palui and Anshika Kapur for fruitful discussions.

■ REFERENCES

- (1) Jain, P. K.; Huang, X. H.; El-Sayed, I. H.; El-Sayed, M. A. Noble Metals on the Nanoscale: Optical and Photothermal Properties and Some Applications in Imaging, Sensing, Biology, and Medicine. *Acc. Chem. Res.* **2008**, *41*, 1578–1586.
- (2) Grzelczak, M.; Perez-Juste, J.; Mulvaney, P.; Liz-Marzan, L. M. Shape Control in Gold Nanoparticle Synthesis. *Chem. Soc. Rev.* **2008**, *37*, 1783–1791.
- (3) Yang, X.; Yang, M. X.; Pang, B.; Vara, M.; Xia, Y. N. Gold Nanomaterials at Work in Biomedicine. *Chem. Rev.* **2015**, *115*, 10410–10488.
- (4) Near, R. D.; Hayden, S. C.; Hunter, R. E.; Thackston, D.; El-Sayed, M. A. Rapid and Efficient Prediction of Optical Extinction Coefficients for Gold Nanospheres and Gold Nanorods. *J. Phys. Chem. C* **2013**, *117*, 23950–23955.
- (5) Dreaden, E. C.; Alkilany, A. M.; Huang, X. H.; Murphy, C. J.; El-Sayed, M. A. The Golden Age: Gold Nanoparticles for Biomedicine. *Chem. Soc. Rev.* **2012**, *41*, 2740–2779.
- (6) Dulkeith, E.; Morteani, A. C.; Niedereichholz, T.; Klar, T. A.; Feldmann, J.; Levi, S. A.; van Veggel, F. C.; Reinhoudt, D. N.; Möller, M.; Gittins, D. I. Fluorescence Quenching of Dye Molecules near Gold Nanoparticles: Radiative and Nonradiative Effects. *Phys. Rev. Lett.* **2002**, *89*, 203002.
- (7) Abadeer, N. S.; Brennan, M. R.; Wilson, W. L.; Murphy, C. J. Distance and Plasmon Wavelength Dependent Fluorescence of Molecules Bound to Silica-Coated Gold Nanorods. *ACS Nano* **2014**, *8*, 8392–8406.
- (8) Giljohann, D. A.; Seferos, D. S.; Daniel, W. L.; Massich, M. D.; Patel, P. C.; Mirkin, C. A. Gold Nanoparticles for Biology and Medicine. *Angew. Chem., Int. Ed.* **2010**, *49*, 3280–3294.
- (9) Nam, J.; Won, N.; Bang, J.; Jin, H.; Park, J.; Jung, S.; Jung, S.; Park, Y.; Kim, S. Surface Engineering of Inorganic Nanoparticles for Imaging and Therapy. *Adv. Drug Delivery Rev.* **2013**, *65*, 622–648.
- (10) Howes, P. D.; Chandrawati, R.; Stevens, M. M. Colloidal Nanoparticles as Advanced Biological Sensors. *Science* **2014**, *346*, 1247390.
- (11) Palui, G.; Aldeek, F.; Wang, W. T.; Mattoussi, H. Strategies for Interfacing Inorganic Nanocrystals with Biological Systems Based on Polymer-Coating. *Chem. Soc. Rev.* **2015**, *44*, 193–227.
- (12) Saha, K.; Agasti, S. S.; Kim, C.; Li, X. N.; Rotello, V. M. Gold Nanoparticles in Chemical and Biological Sensing. *Chem. Rev.* **2012**, *112*, 2739–2779.
- (13) Ji, X.; Wang, W. T.; Mattoussi, H. Controlling the Spectroscopic Properties of Quantum Dots Via Energy Transfer and Charge Transfer Interactions: Concepts and Applications. *Nano Today* **2016**, *11*, 98–121.
- (14) Cobley, C. M.; Chen, J.; Cho, E. C.; Wang, L. V.; Xia, Y. Gold Nanostructures: A Class of Multifunctional Materials for Biomedical Applications. *Chem. Soc. Rev.* **2011**, *40*, 44–56.
- (15) Mattoussi, H.; Palui, G.; Na, H. B. Luminescent Quantum Dots as Platforms for Probing *In Vitro* and *In Vivo* Biological Processes. *Adv. Drug Delivery Rev.* **2012**, *64*, 138–166.
- (16) Mout, R.; Moyano, D. F.; Rana, S.; Rotello, V. M. Surface Functionalization of Nanoparticles for Nanomedicine. *Chem. Soc. Rev.* **2012**, *41*, 2539–2544.

- (17) Mizuhara, T.; Moyano, D. F.; Rotello, V. M. Using the Power of Organic Synthesis for Engineering the Interactions of Nanoparticles with Biological Systems. *Nano Today* **2016**, *11*, 31–40.
- (18) Rouhana, L. L.; Jaber, J. A.; Schlenoff, J. B. Aggregation-Resistant Water-Soluble Gold Nanoparticles. *Langmuir* **2007**, *23*, 12799–12801.
- (19) Garcia, I.; Sanchez-Iglesias, A.; Henriksen-Lacey, M.; Grzelczak, M.; Penades, S.; Liz-Marzan, L. M. Glycans as Biofunctional Ligands for Gold Nanorods: Stability and Targeting in Protein-Rich Media. *J. Am. Chem. Soc.* **2015**, *137*, 3686–3692.
- (20) Stewart, M. H.; Susumu, K.; Mei, B. C.; Medintz, I. L.; Delehanty, J. B.; Blanco-Canosa, J. B.; Dawson, P. E.; Mattoussi, H. Multidentate Poly(Ethylene Glycol) Ligands Provide Colloidal Stability to Semiconductor and Metallic Nanocrystals in Extreme Conditions. *J. Am. Chem. Soc.* **2010**, *132*, 9804–9813.
- (21) Mei, B. C.; Susumu, K.; Medintz, I. L.; Delehanty, J. B.; Mountziaris, T. J.; Mattoussi, H. Modular Poly(Ethylene Glycol) Ligands for Biocompatible Semiconductor and Gold Nanocrystals with Extended Ph and Ionic Stability. *J. Mater. Chem.* **2008**, *18*, 4949–4958.
- (22) Niidome, T.; Yamagata, M.; Okamoto, Y.; Akiyama, Y.; Takahashi, H.; Kawano, T.; Katayama, Y.; Niidome, Y. Peg-Modified Gold Nanorods with a Stealth Character for in Vivo Applications. *J. Controlled Release* **2006**, *114*, 343–347.
- (23) Liu, M.; Law, W.-C.; Kopwithaya, A.; Liu, X.; Swihart, M. T.; Prasad, P. N. Exploring the Amphiphilicity of Pegylated Gold Nanorods: Mechanical Phase Transfer and Self-Assembly. *Chem. Commun.* **2013**, *49*, 9350–9352.
- (24) Moyano, D. F.; Saha, K.; Prakash, G.; Yan, B.; Kong, H.; Yazdani, M.; Rotello, V. M. Fabrication of Corona-Free Nanoparticles with Tunable Hydrophobicity. *ACS Nano* **2014**, *8*, 6748–6755.
- (25) Jiang, Y.; Huo, S.; Mizuhara, T.; Das, R.; Lee, Y. W.; Hou, S.; Moyano, D. F.; Duncan, B.; Liang, X. J.; Rotello, V. M. The Interplay of Size and Surface Functionality on the Cellular Uptake of Sub-10 Nm Gold Nanoparticles. *ACS Nano* **2015**, *9*, 9986–9993.
- (26) Zhang, F.; Lees, E.; Amin, F.; Rivera-Gil, P. R.; Yang, F.; Mulvaney, P.; Parak, W. J. Polymer-Coated Nanoparticles: A Universal Tool for Biolabelling Experiments. *Small* **2011**, *7*, 3113–3127.
- (27) Aldana, J.; Wang, Y. A.; Peng, X. Photochemical Instability of Cdse Nanocrystals Coated by Hydrophilic Thiols. *J. Am. Chem. Soc.* **2001**, *123*, 8844–8850.
- (28) Wang, W.; Kapur, A.; Ji, X.; Safi, M.; Palui, G.; Palomo, V.; Dawson, P. E.; Mattoussi, H. Photoligation of an Amphiphilic Polymer with Mixed Coordination Provides Compact and Reactive Quantum Dots. *J. Am. Chem. Soc.* **2015**, *137*, 5438–5451.
- (29) Yang, W.; Zhang, L.; Wang, S.; White, A. D.; Jiang, S. Functionalizable and Ultra Stable Nanoparticles Coated with Zwitterionic Poly(Carboxybetaine) in Undiluted Blood Serum. *Biomaterials* **2009**, *30*, 5617–5621.
- (30) Kang, J. S.; Taton, T. A. Oligothiol Graft-Copolymer Coatings Stabilize Gold Nanoparticles against Harsh Experimental Conditions. *Langmuir* **2012**, *28*, 16751–16760.
- (31) Liu, X.; Huang, H.; Liu, G.; Zhou, W.; Chen, Y.; Jin, Q.; Ji, J. Multidentate Zwitterionic Chitosan Oligosaccharide Modified Gold Nanoparticles: Stability, Biocompatibility and Cell Interactions. *Nanoscale* **2013**, *5*, 3982–3991.
- (32) Chen, X.; Lawrence, J.; Parekar, S.; Emrick, T. Novel Zwitterionic Copolymers with Dihydrolipoic Acid: Synthesis and Preparation of Nonfouling Nanorods. *Macromolecules* **2013**, *46*, 119–127.
- (33) Liu, X.; Huang, N.; Li, H.; Wang, H.; Jin, Q.; Ji, J. Multidentate Polyethylene Glycol Modified Gold Nanorods for in Vivo near-Infrared Photothermal Cancer Therapy. *ACS Appl. Mater. Interfaces* **2014**, *6*, 5657–5668.
- (34) Wang, W.; Aldeek, F.; Ji, X.; Zeng, B.; Mattoussi, H. A Multifunctional Amphiphilic Polymer as a Platform for Surface-Functionalizing Metallic and Other Inorganic Nanostructures. *Faraday Discuss.* **2014**, *175*, 137–151.
- (35) Wang, W.; Ji, X.; Burns, H.; Mattoussi, H. A Multi-Coordinating Polymer Ligand Optimized for the Functionalization of Metallic Nanocrystals and Nanorods. *Faraday Discuss.* **2016**, *191*, 481–494.
- (36) Susumu, K.; Mei, B. C.; Mattoussi, H. Multifunctional Ligands Based on Dihydrolipoic Acid and Polyethylene Glycol to Promote Biocompatibility of Quantum Dots. *Nat. Protoc.* **2009**, *4*, 424–436.
- (37) Wang, W.; Kapur, A.; Ji, X.; Zeng, B.; Mishra, D.; Mattoussi, H. Multifunctional and High Affinity Polymer Ligand That Provides Bio-Orthogonal Coating of Quantum Dots. *Bioconjugate Chem.* **2016**, *27*, 2024–2036.
- (38) Enustun, B. V.; Turkevich, J. Coagulation of Colloidal Gold. *J. Am. Chem. Soc.* **1963**, *85*, 3317–3328.
- (39) Schwartzberg, A. M.; Olson, T. Y.; Talley, C. E.; Zhang, J. Z. Synthesis, Characterization, and Tunable Optical Properties of Hollow Gold Nanospheres. *J. Phys. Chem. B* **2006**, *110*, 19935–19944.
- (40) Ye, X. C.; Jin, L. H.; Caglayan, H.; Chen, J.; Xing, G. Z.; Zheng, C.; Doan-Nguyen, V.; Kang, Y. J.; Engheta, N.; Kagan, C. R.; et al. Improved Size-Tunable Synthesis of Monodisperse Gold Nanorods through the Use of Aromatic Additives. *ACS Nano* **2012**, *6*, 2804–2817.
- (41) Pons, T.; Uyeda, H. T.; Medintz, I. L.; Mattoussi, H. Hydrodynamic Dimensions, Electrophoretic Mobility, and Stability of Hydrophilic Quantum Dots. *J. Phys. Chem. B* **2006**, *110*, 20308–20316.
- (42) Berne, B. J.; Pecora, R. *Dynamic Light Scattering: With Applications to Chemistry, Biology, and Physics*; Dover Publications: Mineola, NY, 2000.
- (43) Schärfl, W. *Light Scattering from Polymer Solutions and Nanoparticle Dispersions*; Springer Laboratory Manuals in Polymer Science; Springer: Berlin, 2007; pp 1–191.
- (44) Mattoussi, H.; Cumming, A. W.; Murray, C. B.; Bawendi, M. G.; Ober, R. Properties of Cdse Nanocrystal Dispersions in the Dilute Regime: Structure and Interparticle Interactions. *Phys. Rev. B: Condens. Matter Mater. Phys.* **1998**, *58*, 7850–7863.
- (45) Mattoussi, H.; Karasz, F. E.; Langley, K. H. Electrostatic and Screening Effects on the Dynamic Aspects of Polyelectrolyte Solutions. *J. Chem. Phys.* **1990**, *93*, 3593–3603.
- (46) Wang, W.; Ji, X.; Na, H. B.; Safi, M.; Smith, A.; Palui, G.; Perez, J. M.; Mattoussi, H. Design of a Multi-Dopamine-Modified Polymer Ligand Optimally Suited for Interfacing Magnetic Nanoparticles with Biological Systems. *Langmuir* **2014**, *30*, 6197–6208.
- (47) Turkevich, J.; Stevenson, P. C.; Hillier, J. A Study of the Nucleation and Growth Processes in the Synthesis of Colloidal Gold. *Discuss. Faraday Soc.* **1951**, *11*, 55–75.
- (48) Li, J.; Zhou, M.; Liu, F.; Xiong, C.; Wang, W.; Cao, Q.; Wen, X.; Robertson, J. D.; Ji, X.; Wang, Y. A.; et al. Hepatocellular Carcinoma: Intra-Arterial Delivery of Doxorubicin-Loaded Hollow Gold Nanospheres for Photothermal Ablation—Chemoembolization Therapy in Rats. *Radiology* **2016**, *281*, 427–435.
- (49) Mahmoudi, M.; Lynch, I.; Ejtehadi, M. R.; Monopoli, M. P.; Bombelli, F. B.; Laurent, S. Protein-Nanoparticle Interactions: Opportunities and Challenges. *Chem. Rev.* **2011**, *111*, 5610–5637.
- (50) Salvati, A.; Pitek, A. S.; Monopoli, M. P.; Prapainop, K.; Bombelli, F. B.; Hristov, D. R.; Kelly, P. M.; Aberg, C.; Mahon, E.; Dawson, K. A. Transferrin-Functionalized Nanoparticles Lose Their Targeting Capabilities When a Biomolecule Corona Adsorbs on the Surface. *Nat. Nanotechnol.* **2013**, *8*, 137–143.
- (51) Pelaz, B.; del Pino, P.; Maffre, P.; Hartmann, R.; Gallego, M.; Rivera-Fernández, S.; de la Fuente, J. M.; Nienhaus, G. U.; Parak, W. J. Surface Functionalization of Nanoparticles with Polyethylene Glycol: Effects on Protein Adsorption and Cellular Uptake. *ACS Nano* **2015**, *9*, 6996–7008.
- (52) Welscher, K.; McManus, S. A.; Hsia, C.-H.; Yin, S.; Yang, H. Discovery of Protein- and DNA-Imperceptible Nanoparticle Hard Coating Using Gel-Based Reaction Tuning. *J. Am. Chem. Soc.* **2015**, *137*, 580–583.
- (53) Schöttler, S.; Becker, G.; Winzen, S.; Steinbach, T.; Mohr, K.; Landfester, K.; Mailänder, V.; Wurm, F. R. Protein Adsorption Is Required for Stealth Effect of Poly(Ethylene Glycol)- and Poly-

(Phosphoester)-Coated Nanocarriers. *Nat. Nanotechnol.* **2016**, *11*, 372–377.

(54) Docter, D.; Westmeier, D.; Markiewicz, M.; Stolte, S.; Knauer, S. K.; Stauber, R. H. The Nanoparticle Biomolecule Corona: Lessons Learned - Challenge Accepted? *Chem. Soc. Rev.* **2015**, *44*, 6094–6121.

(55) Lynch, I.; Dawson, K. A. Protein-Nanoparticle Interactions. *Nano Today* **2008**, *3*, 40–47.

(56) Burtis, C. A.; Ashwood, E. R.; Bruns, D. E.; Tietz, N. W. *Tietz Textbook of Clinical Chemistry and Molecular Diagnostics*, 5th ed.; Saunders: St. Louis, MO, 2013.

(57) Wang, W.; Ji, X.; Kapur, A.; Zhang, C.; Mattoussi, H. A Multifunctional Polymer Combining the Imidazole and Zwitterion Motifs as a Biocompatible Compact Coating for Quantum Dots. *J. Am. Chem. Soc.* **2015**, *137*, 14158–14172.

(58) Mei, B. C.; Oh, E.; Susumu, K.; Farrell, D.; Mountziaris, T. J.; Mattoussi, H. Effects of Ligand Coordination Number and Surface Curvature on the Stability of Gold Nanoparticles in Aqueous Solutions. *Langmuir* **2009**, *25*, 10604–10611.

(59) Weisbecker, C. S.; Merritt, M. V.; Whitesides, G. M. Molecular Self-Assembly of Aliphatic Thiols on Gold Colloids. *Langmuir* **1996**, *12*, 3763–3772.

(60) Agasti, S. S.; You, C.-C.; Arumugam, P.; Rotello, V. M. Structural Control of the Monolayer Stability of Water-Soluble Gold Nanoparticles. *J. Mater. Chem.* **2008**, *18*, 70–73.